

Structural features of the endocardium, arteries, prostate and adrenal glands under the conditions of iodine deficiency

Liliia V. Sobol, Ivan S. Kuibida, Oleksandra T. Harhaun, Oksana H. Popadynets

IVANO-FRANKIVSK NATIONAL MEDICAL UNIVERSITY, IVANO-FRANKIVSK, UKRAINE

ABSTRACT

Aim: To trace morphofunctional changes in the endocardium, arterial walls of various types, prostate gland, and adrenal gland during iodine deficiency in postnatal ontogenesis.

Materials and Methods: The experiment involved 50 male Wistar rats (25 immature, aged 3-5 months, and 25 mature, aged 6-8 months). Group 1 (control) included 11 animals of both age groups, while Groups 2 and 3 (with iodine deficiency) consisted of 14 animals each, with material sampling on days 60 and 90 of the experiment, respectively. Morphological (light and electron microscopy), morphometric, biochemical studies, and statistical data processing were conducted.

Results: The frequency of cardiovascular system damage, lesions of the prostate and adrenal glands, and iodine deficiency are important to study because of influence to the thyroid imbalance on these organs. The aim was to indicate the morphofunctional changes in the endocardium, wall of the arteries of various types, prostate gland, and adrenal glands in the dynamics of iodine deficiency during postnatal ontogenesis. Key components of thyroid signaling were found in the prostate gland, indicating a possible direct effect of thyroid hormones on this organ. Edematous changes in the epithelium of terminal secretory parts result from ischemia caused by edema in vascular walls and connective tissue elements of the prostate. Structural changes found in endocrine cells of the glomerular, fascicular, and reticular zones of the adrenal glands, along with the dynamic increase in cortical thickness during the experiment, suggest trophic disturbances, as edema was detected in vessel walls and stromal components. Thus, on both day 60 and day 90 of iodine deficiency, edematous changes occur in all organs in connective tissue components, wall of blood vessels, and epithelial tissues. Altered thyroid status triggers systemic interrelated changes in the organism.

Conclusions: On both day 60 and day 90 of iodine deficiency, edematous changes occur in all organs in connective tissue components, wall of blood vessels, and epithelial tissues. Altered thyroid status triggers systemic interrelated changes in the organism.

KEY WORDS: endocardium, arteries, prostate gland, adrenal gland, iodine deficiency, structural-metabolic disorders, ontogenesis

Wiad Lek. 2025;78(10):1981-1987. doi: 10.36740/WLek/213591 DOI

INTRODUCTION

The basis of alimentary hypothyroidism lies in the biogeochemical features of specific regions where iodine levels are reduced [1-5]. Thyroid hormones, which include iodine, regulate energy homeostasis, and even minor reductions in their levels increase the risk of cardiovascular diseases [6-9]. Under iodine deficiency, cardiovascular dysfunction develops asymptotically [10-13]. Thyroid hormones are essential for the development of reproductive organs. Their deficiency during critical growth periods alters the size and function of the prostate gland in adulthood [14]. Hypothyroidism is known to reduce adrenal gland weight and plasma corticosterone concentration [15]. While a connection between these organs and the thyroid gland is evident, there is no comprehensive study on the impact of iodine deficiency on their morphofunctional state considering age-specific features.

AIM

To trace morphofunctional changes in the endocardium, arterial walls of various types, prostate gland, and adrenal gland during iodine deficiency in postnatal ontogenesis.

MATERIALS AND METHODS

Samples from the endocardium, fragments of the aorta, external carotid, and renal arteries, prostate gland (ventral, dorsal lobes, and coagulating gland), adrenal glands, blood, and urine were analyzed. Iodine deficiency was modeled using a specific methodology [2]. All procedures adhered strictly to humane treatment of animals. The experiment involved 50 male Wistar rats (25 immature, aged 3-5 months, and 25 mature, aged 6-8 months). Group 1 (control) included 11 animals of both age groups, while Groups 2 and 3 (with iodine

deficiency) consisted of 14 animals each, with material sampling on days 60 and 90 of the experiment, respectively. Morphological (light and electron microscopy), morphometric, biochemical studies, and statistical data processing were conducted [16].

FRAMEWORK

The study is carried out within the framework of the initiative research work of the Department of Human Anatomy at Ivano-Frankivsk National Medical University "Ontogenetic Peculiarities of the Morpho-functional State of Organs and Tissues in Iodine Deficiency and Hypothyroidism" (0119U002847).

RESULTS

The thyroid status of immature animals in Group 1 was as follows: TSH 0.10 ± 0.01 μ U/ml ($p < 0.01$), T3 3.63 ± 0.12 nmol/l ($p < 0.01$), T4 75.44 ± 4.01 nmol/l ($p < 0.01$); for mature animals, TSH was 0.08 ± 0.00 μ U/ml ($p < 0.01$), T3 2.79 ± 0.15 nmol/l ($p < 0.01$), T4 55.18 ± 2.72 nmol/l ($p < 0.01$). Cholesterol content under age norm conditions was 1.60 ± 0.05 mmol/l ($p < 0.01$) in immature rats and 1.40 ± 0.09 mmol/l ($p < 0.01$) in mature rats. Ioduria in immature animals of Group 1 was 97.13 ± 5.40 μ g/l, and in mature animals – 101.06 ± 3.44 μ g/l ($p < 0.01$).

Thyroid status of immature animals in Group 2 showed TSH 0.17 ± 0.02 μ U/ml ($p < 0.01$), T3 3.46 ± 0.36 nmol/l ($p < 0.01$), T4 75.49 ± 9.60 nmol/l ($p < 0.01$); in mature animals, TSH was 0.12 ± 0.01 μ U/ml ($p < 0.01$), T3 2.97 ± 0.37 nmol/l ($p < 0.01$), T4 67.49 ± 8.25 nmol/l ($p < 0.01$). Cholesterol on day 60 of the experiment was 1.63 ± 0.17 mmol/l ($p < 0.01$) in immature rats and 1.39 ± 0.12 mmol/l ($p < 0.01$) in mature rats. Ioduria in immature animals of Group 2 was 2.73 ± 0.29 μ g/l, and in mature animals – 3.77 ± 0.34 μ g/l ($p < 0.01$).

On day 60 of iodine deficiency, the endocardium appeared as a thin eosinophilic strip with well-defined oval nuclei; in some loci, nuclei were round. Ultrastructurally, the luminal plasmalemma of endothelial cells formed numerous invaginations. Membrane organelles were swollen. The subendothelial layer contained an amorphous substance of medium electron density. Mitochondria and endoplasmic reticulum were identified in the smooth muscle cells of the muscular-elastic layer (Fig. 1). Endothelin-1 blood levels in immature animals increased by 2.9% ($p < 0.05$), while no change was observed in mature animals.

In the walls of elastic, muscular and muscular-elastic arteries, all layers were identified, but the contour of their lumen was changed due to uneven twists of the

connective tissue framework. The endothelial layer of the intima was light, endothelial nuclei were not visible in all fields of view. The nuclei of smooth muscle cells were oriented in various directions with differing degrees of basophilia. The adventitia was blurred.

Ultrastructurally, endothelial cells showed organelle swelling and multiple luminal plasmalemma invaginations. The internal elastic membrane had loci of luminalization. Sarcoplasm of smooth muscle cells had a granular-fibrillar structure.

Morphometric analysis showed that in immature animals, the thickness of the aortic, external carotid, and renal artery walls increased by 0.9% ($p < 0.05$), 0.9% ($p < 0.05$), and 0.6% ($p < 0.05$), respectively. In mature animals, the thickness increased by 0.2% ($p < 0.05$), 0.7% ($p < 0.05$), and 1.1% ($p < 0.05$), respectively.

At this stage of the experiment, edema was observed in the connective tissue elements of the stroma and wall of blood vessels in all parts of the prostate gland (ventral, dorsal, and coagulating glands) (Fig. 2). Epithelial cells of terminal secretory parts had apically light cytoplasm and basal basophilia of nuclear poles. Ultrastructurally, nuclei contained euchromatin and a thin band of heterochromatin. Granular endoplasmic reticulum tubules were dilated, and Golgi apparatus cisternae unevenly filled the cytoplasm. Mitochondrial matrix was of low electron density; cristae were disorganized. Secretory granules varied in shape and size. The height of the epithelium in the terminal secretory parts of the ventral, dorsal lobes, and coagulating glands increased by 0.3% ($p < 0.05$), 0.7% ($p < 0.05$), and 0.9% ($p < 0.05$) in immature animals, respectively. In mature animals, epithelium height increased by 0.2% ($p < 0.05$), 0.4% ($p < 0.05$), and 0.9% ($p < 0.05$), respectively.

In the adrenal glands, light microscopy showed edema of the capsule (Fig. 2C). Zona glomerulosa was represented by basophilic-stained endocrine cells; in zona fasciculata, cells were weakly eosinophilic, with more intense eosinophilia in zona reticularis. In all zones of the cortex and in medulla, blood vessel lumens and networks were visible. Submicroscopically, pericellular luminal loci were visible (Fig. 2D). Endocrinocytes showed invagination of the nuclear envelope and marginal chromatin localization. Membrane organelles were swollen. Secretory granules had medium electron density. Cortical thickness of adrenal glands in immature animals increased by 0.4% ($p < 0.05$), and in mature animals by 1.5% ($p < 0.05$).

Thyroid status of immature animals in Group 3: TSH 0.16 ± 0.02 μ U/ml ($p < 0.01$), T3 3.47 ± 0.39 nmol/l ($p < 0.01$), T4 51.31 ± 6.53 nmol/l ($p < 0.01$); in mature animals: TSH 0.23 ± 0.03 μ U/ml ($p < 0.01$), T3 2.43 ± 0.29 nmol/l ($p < 0.01$), T4 54.91 ± 7.05 nmol/l ($p < 0.01$).

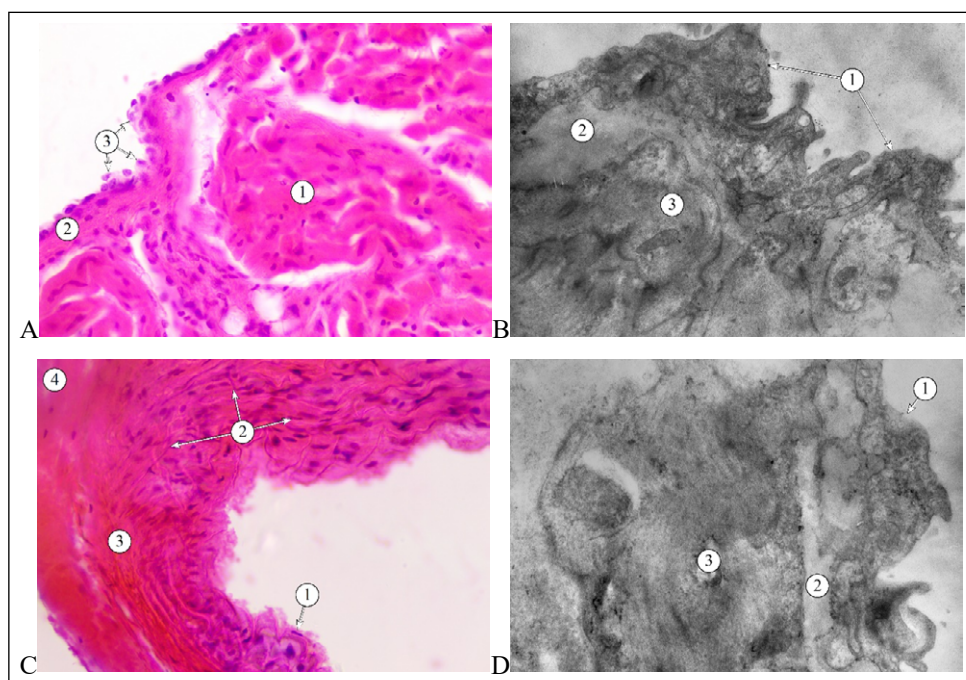


Fig. 1. Structure of the endocardium and arterial walls on day 60 of iodine deficiency.

A. Endocardium of a mature animal: 1 – myocardium, 2 – endocardium, 3 – endothelial cell nuclei.

B. Endocardium of an immature animal: 1 – endothelial cells, 2 – subendothelial layer, 3 – muscular-elastic layer connective tissue

C. Wall of renal artery in immature animal: 1 – endothelial cells, 2 – connective tissue fibers of media, 3 – smooth muscle cells of media, 4 – adventitia.

D. Wall of external carotid artery in mature animal: 1 – endothelial cell, 2 – internal elastic membrane, 3 – smooth muscle cell.

A, C – hematoxylin and eosin, magnification: A, C $\times 400$. B, D – electron micrograph, magnification: B $\times 9600$, D $\times 16000$

Picture taken by the authors

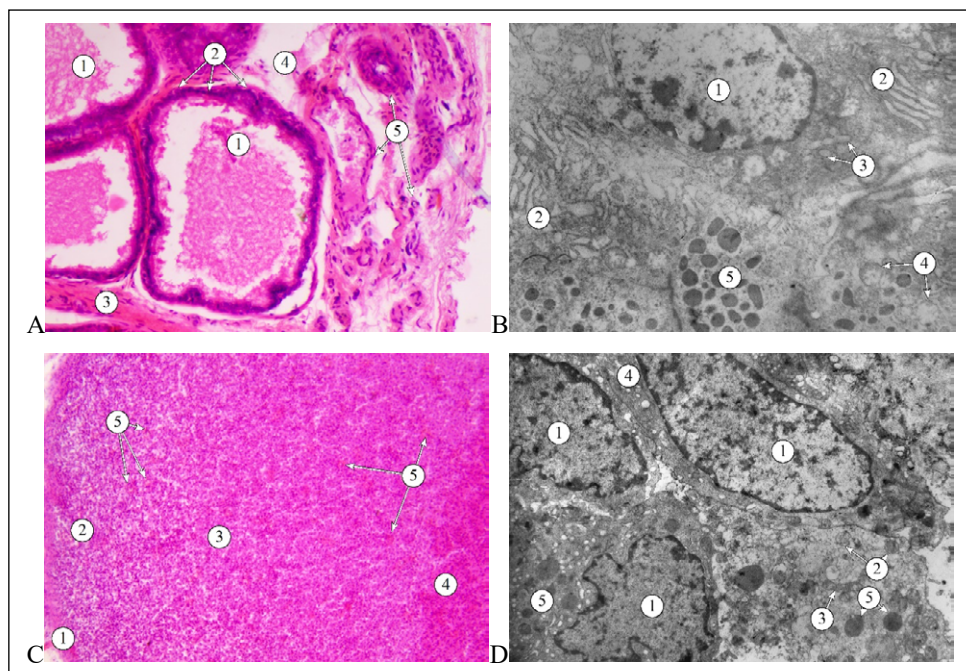


Fig. 2. Structure of the prostate and adrenal glands on day 60 of iodine deficiency

A. Dorsal lobe of prostate gland in mature animal: 1 – terminal secretory parts, 2 – epithelial nuclei, 3 – smooth muscle cells, 4 – connective tissue fibers, 5 – blood vessels

B. Ventral lobe of prostate gland in immature animal: 1 – nucleus, 2 – granular endoplasmic reticulum, 3 – Golgi apparatus, 4 – mitochondria, 5 – secretory granules

C. Adrenal gland of immature animal: 1 – capsule, 2 – zona glomerulosa, 3 – zona fasciculata, 4 – zona reticularis, 5 – blood vessels

D. Endocrine cells of zona glomerulosa adrenal cortex in mature animal: 1 – nucleus, 2 – mitochondria, 3 – endoplasmic reticulum, 4 – Golgi apparatus, 5 – granules

A, C – hematoxylin and eosin, magnification: A $\times 200$, C $\times 100$. B, D – electron micrograph, magnification: B, D $\times 4800$

Picture taken by the authors

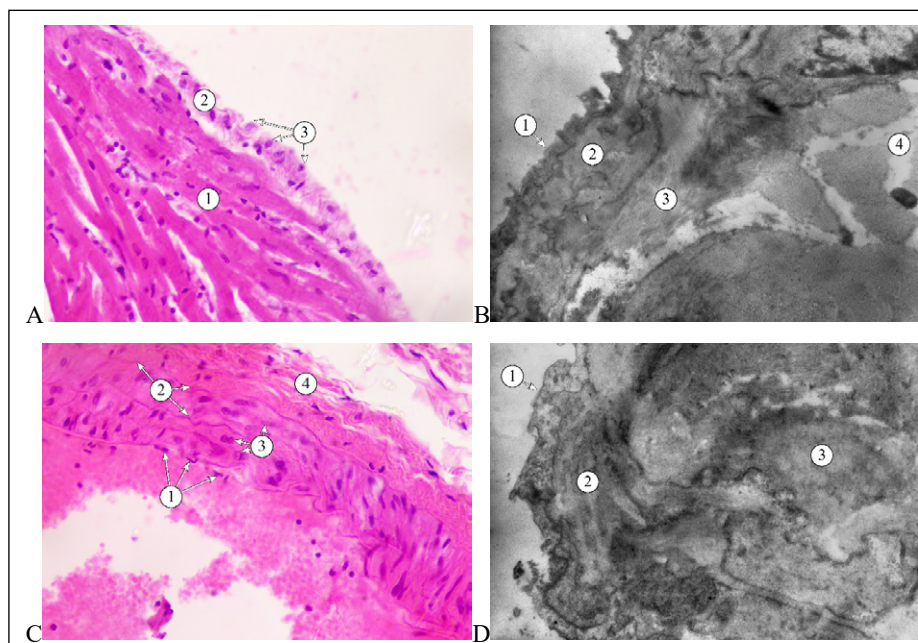


Fig. 3. Structure of the endocardium and wall of the arteries on day 90 of iodine deficiency

A. Endocardium of a mature animal: 1 – myocardium, 2 – endocardium, 3 – endothelial cell nuclei

B. Endocardium of an immature animal: 1 – endothelial cells, 2 – subendothelial layer, 3 – connective tissue fibers of the muscular-elastic layer, 4 – substance of the muscular-elastic layer

C. Wall of renal artery of mature animal: 1 – endothelial cell nuclei, 2 – connective tissue fibers of the media, 3 – smooth muscle cells of the media, 4 – adventitia

D. Wall of aorta of mature animal: 1 – endothelial cell, 2 – subendothelial layer, 3 – smooth muscle cell

A, C – hematoxylin and eosin, magnification: A, C $\times 400$. B, D – electron micrograph, magnification: B $\times 4800$, D $\times 9600$

Picture taken by the authors

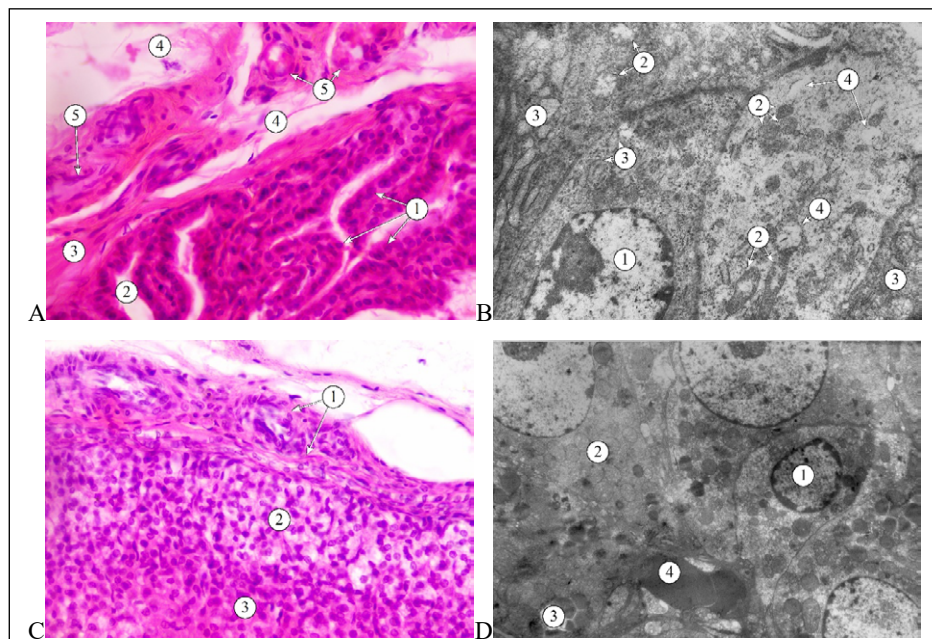


Fig. 4. Structure of prostate and adrenal glands on day 90 of iodine deficiency

A. Coagulating gland of immature animal prostate: 1 – epithelial cells, 2 – lumen of terminal secretory parts, 3 – smooth muscle cells, 4 – connective tissue fibers, 5 – blood vessels

B. Dorsal lobe of mature animal prostate: 1 – nucleus, 2 – mitochondria, 3 – granular endoplasmic reticulum, 4 – vacuoles

C. Adrenal gland of mature animal: 1 – capsule, 2 – zona glomerulosa, 3 – zona fasciculata

D. Endocrine cells of zona fasciculata adrenal cortex in immature animal: 1 – nucleus, 2 – mitochondria, 3 – lipid inclusions, 4 – erythrocyte sludge

A, C – hematoxylin and eosin, magnification: A, C $\times 400$. B, D – electron micrograph, magnification: B $\times 6400$, D $\times 3200$

Picture taken by the authors

Cholesterol content on day 90 of the experiment was 1.66 ± 0.20 mmol/l ($p < 0.01$) in immature rats, and 1.44 ± 0.16 mmol/l ($p < 0.01$) in mature rats. Ioduria in immature animals of Group 3 was 1.89 ± 0.24 μ g/l, and in mature animals 2.29 ± 0.21 μ g/l ($p < 0.01$).

On day 90 of the experiment, the endocardium appeared as an unevenly swollen strip with a cleared subendothelial layer (Fig. 3). The endothelial cell nuclei showed varying intensities of basophilia and were located at different levels. The cytoplasm had a reticular structure. Ultrastructurally, endothelial cells had medium electron density with poorly differentiated organelles. A swollen subendothelial layer was visible, appearing as a homogeneously deformed strip. In the muscular-elastic layer, swollen, differently oriented collagen fibers were found, surrounded by a cleared amorphous substance. Endothelin-1 levels in the blood of immature animals increased by 4.3% ($p < 0.05$), and in mature animals, it increased by 1.2% ($p < 0.05$).

When examining arterial walls, frequent adhesion of formed elements obscuring endothelial cells was observed. The collagen-elastic framework was deformed and swollen. Smooth muscle cell nuclei in the media were oriented in different directions. The adventitia consisted of layered fibers in swollen amorphous material. Submicroscopically, endothelial cells rested on a thin basal membrane. Their luminal surface had a blurred contour along the vessel perimeter. The cytoplasm was diffusely granular with alternating optical lighting. The subendothelial layer had low electron density. Elastic and collagen fibers of the arterial wall were swollen and fragmented. Sarcoplasm of smooth muscle cells was light. Morphometric analysis showed that in immature animals, the thickness of the aorta, external carotid, and renal artery walls increased by 1.0% ($p < 0.05$), 1.2% ($p < 0.05$), and 0.8% ($p < 0.05$), respectively. In mature animals, these parameters increased by 0.6% ($p < 0.05$), 1.3% ($p < 0.05$), and 1.7% ($p < 0.05$), respectively.

The epithelium of the terminal secretory parts of all prostate lobes was swollen (Fig. 4). Nuclei had blurred contours. The cytoplasm was eosinophilic. Edematous connective tissue fibers, amorphous substances, and smooth muscle cells of the gland stroma were noted. Similar edematous changes were present in the walls of blood vessels. Submicroscopically, cytoplasmic lighting of epithelial cells was observed. Granular endoplasmic reticulum tubules were dilated, and the Golgi apparatus consisted of deformed cisternae and tubules. Mitochondria had disorganized cristae and cleared matrix. The height of the epithelium in the terminal secretory parts of the ventral, dorsal lobes, and coagulating glands increased by 3.6% ($p < 0.05$) in immature animals. In mature animals, the height of the epithelium increased by 1.1% ($p < 0.05$), 0.9% ($p < 0.05$), and 1.4% ($p < 0.05$), respectively.

In the adrenal glands, edema was observed in the capsule and parenchyma. Stromal components were layered and deformed, surrounding the swollen walls of blood vessels, whose lumens were changed (Fig. 4C). Prominent pericellular luminalization lightening was seen in all zones of the adrenal cortex and in the medulla. Edematous processes in adrenal endocrinocytes were confirmed by electron microscopy (Fig. 4D). Mitochondrial matrix was dispersed and of low electron density, with disorganized cristae. Secretory granules were heterogeneous and sparse. Blood vessels showed stasis phenomena. The thickness of the adrenal cortical layer increased by 1.4% ($p < 0.05$) in immature animals and by 2.4% ($p < 0.05$) in mature animals.

DISCUSSION

Thyroid hormones influence cellular oxygen metabolism [6, 7, 17]. They maintain vascular homeostasis through positive effects on endothelial cells and smooth muscle cells of blood vessels [18]. According to our data, endothelin-1 levels slightly increased by day 60 of iodine deficiency with further rise by day 90. Endothelin-1 is a potent vasoconstrictor [19, 20]. The observed edematous changes in vascular walls correlate with other authors' findings on decreased elasticity and increased vascular resistance [21–23]. Endothelial dysfunction worsens due to impaired lipid metabolism under iodine deficiency [24, 25].

According to our data, cholesterol content changes serve as a marker of this. It is known that structural changes in the endocardium are associated with elevated cholesterol levels, indicating the impact of iodine deficiency on thyroid hormones and metabolism, thus increasing the risk of cardiovascular diseases [12, 26].






Key components of thyroid signaling were found in the prostate gland, indicating a possible direct effect of thyroid hormones on this organ [14]. Edematous changes in the epithelium of terminal secretory parts result from ischemia caused by edema in vascular walls and connective tissue elements of the prostate [27, 28]. Structural changes found in endocrine cells of the glomerular, fascicular, and reticular zones of the adrenal glands, along with the dynamic increase in cortical thickness during the experiment, suggest trophic disturbances, as edema was detected in vessel walls and stromal components.

CONCLUSIONS

Thus, on both day 60 and day 90 of iodine deficiency, edematous changes occur in all organs in connective tissue components, wall of blood vessels, and epithelial tissues. Altered thyroid status triggers systemic interrelated changes in the organism.

REFERENCES

1. Kerver JM, Pearce EN, Ma T et al. Prevalence of inadequate and excessive iodine intake in a US pregnancy cohort. *Am J Obstet Gynecol*. 2021;224(1):82.e1-82.e8. doi:10.1016/j.ajog.2020.06.052. DOI
2. Martínez-Galán JR, Pedraza P, Santacana M et al. Early effects of iodine deficiency on radial glial cells of the hippocampus of the rat fetus. A model of neurological cretinism. *J Clin Invest*. 1997;99(11):2701-2709. doi:10.1172/jci119459. DOI
3. Moog NK, Entringer S, Heim C et al. Influence of maternal thyroid hormones during gestation on fetal brain development. *Neuroscience*. 2017;342:68-100. doi:10.1016/j.neuroscience.2015.09.070. DOI
4. Niwattisaiwong S, Burman KD, Li-Ng M. Iodine deficiency: clinical implications. *Cleve Clin J Med*. 2017;84(3):236-244. doi:10.3949/ccjm.84a.15053. DOI
5. World Health Organization. Iodine Deficiency. <https://www.who.int/data/nutrition/nlis/info/iodine-deficiency> [Accessed 9 January 2025]
6. Baumgartner C, da Costa BR, Collet TH et al. Thyroid function within the normal range, subclinical hypothyroidism, and the risk of atrial fibrillation. *Circulation*. 2017;136(22):2100-2116. doi:10.1161/CIRCULATIONAHA.117.028753. DOI
7. Blum MR, Gencer B, Adam L et al. Impact of thyroid hormone therapy on atherosclerosis in the elderly with subclinical hypothyroidism: A randomized trial. *J Clin Endocrinol Metab*. 2018;103(8):2988-2997. doi:10.1210/jc.2018-00279. DOI
8. Omid N, Khorgami M, Tajrishi FZ et al. The role of thyroid diseases and their medications in cardiovascular disorders: A review of the literature. *Curr Cardiol Rev*. 2020;16(2):103-116. doi:10.2174/1573403X15666191008111238. DOI
9. Pehrsson PR, Roseland JM, Patterson KY et al. Iodine in foods and dietary supplements: A collaborative database developed by NIH, FDA and USDA. *J Food Compos Anal*. 2022;109:104369. doi:10.1016/j.jfca.2021.104369. DOI
10. Isailă OM, Stoian VE, Fulga I et al. The relationship between subclinical hypothyroidism and carotid intima-media thickness as a potential marker of cardiovascular risk: A systematic review and a meta-analysis. *J Cardiovasc Dev Dis*. 2024;11(4):98. doi:10.3390/jcdd11040098. DOI
11. Kukharchuk KhM. Clinical and epidemiological features of a subclinical hypothyroidism in young people. *Health of Society*. 2019;8(3):106-111. doi:10.22141/2306-2436.8.3.2019.192174. DOI
12. Peixoto de Miranda ÉJF, Bittencourt MS, Pereira AC et al. Subclinical hypothyroidism is associated with higher carotid intima-media thickness in cross-sectional analysis of the Brazilian Longitudinal Study of Adult Health (ELSA-Brasil). *Nutr Metab Cardiovasc Dis*. 2016;26(10):915-921. doi:10.1016/j.numecd.2016.06.005. DOI
13. Sampaio RAG, Riet-Correa F, Barbosa FMS et al. Diffuse alopecia and thyroid atrophy in sheep. *Animals (Basel)*. 2021;11(12):3530. doi:10.3390/ani11123530. DOI
14. Anguiano B, de Oca CM, Delgado-González E, Aceves C. Prostate gland as a target organ of thyroid hormones: advances and controversies. *Endocr Connect*. 2022;11(2):e210581. doi:10.1530/EC-21-0581. DOI
15. Ryabukha O, Greguš M. Correlation analysis as a thyroid gland, adrenal glands, and liver relationship tool for correcting hypothyroidism with organic and inorganic iodine. *Procedia Comput Sci*. 2019;160:598-603. doi:10.1016/j.procs.2019.11.041. DOI
16. Bahrii MM, Dibrova VA, Popadynets OH, Hryshchuk MI. *Metody morfolohichnykh doslidzhen': Monohrafiya*. [Methods of morphological research: A monograph]. Vinnytsia: Nova Knyha. 2016, p.328. (Ukrainian)
17. Hlozyk IZ. Biokhimichni markery vil'noradykal'noho okyslennya ta lipidnoho obminu u shchuriv z ozhyrinnyam, yododefitsytom ta ozhyrinnyam u poyednanni z yododefitsytom. [Biochemical markers of free radical oxidation and lipid exchange in rats with obesity, iodine deficiency and obesity in combination with iodine deficiency]. *Ukrayins'kyi zhurnal medytsyny, biolohiyi ta sportu*. 2021;6(4):166-171. doi:10.26693/jmbs06.04.166. (Ukrainian) DOI
18. Jung KY, Ahn HY, Han SK et al. Association between thyroid function and lipid profiles, apolipoproteins, and high-density lipoprotein function. *J Clin Lipidol*. 2017;11(6):1347-1353. doi:10.1016/j.jacl.2017.08.015. DOI
19. Pankiv VI, Yuzvenko TYu. Relationships of subclinical thyroid dysfunction and metabolic syndrome. *Clin Endocrinol Endocr Surg (Ukraine)*. 2017;2(58):39-43. doi:10.24026/1818-1384.2(58).2017.105577. (Ukrainian) DOI
20. Skrypnyk NV. *Metabolichnyy syndrom ta hipotyreoz: patohenetychni vzayemozv'yazky, diahnozyka ta likuvannya*. [Metabolic syndrome and hypothyroidism: pathogenetic interrelations, diagnosis, and treatment]. *Diabetolohiya, tyreoyidolohiya, metabolichni rozlady*. 2017;1(37):60-63. (Ukrainian)
21. Asín J, Ramírez GA, Navarro MA et al. Nutritional wasting disorders in sheep. *Animals (Basel)*. 2021;11(2):501. doi:10.3390/ani11020501. DOI
22. Hetmaniuk IB, Fedoniuk LYa, Zhulkevych IV et al. Microscopic and submicroscopic structure of the heart atria and auricles in condition of the experimental thermal trauma. *Biointerface Research in Applied Chemistry*. 2020;2(10):5237-5242. doi:10.33263/BRIAC102.237242. DOI
23. Benzar IM, Levytskyi AF, Diehtiarova DS et al. Vascular anomalies in newborns: clinical presentation, complications, and peculiarities of therapy. *Wiad lek*. 2020;9(73):1934-1939. doi:10.36740/WLek202009207. DOI

24. Fabricio MF, Jordão MT, Miotto DS et al. Standardization of a new non-invasive device for assessment of arterial stiffness in rats: Correlation with age-related arteries' structure. *MethodsX*. 2020;7:100901. doi:10.1016/j.mex.2020.100901. DOI 
25. Lindesay G, Bézie Y, Ragonnet C et al. Differential stiffening between the abdominal and thoracic aorta: effect of salt loading in stroke-prone hypertensive rats. *J Vasc Res*. 2018;55(3):144-158. doi:10.1159/000488877. DOI 
26. Ranhulova T. Non-alcoholic fatty liver disease and hypothyroidism: review of clinical and experimental studies. *Galician Medical Journal*. 2021;28(4):E202142. doi:10.21802/gmj.2021.4.2. DOI 
27. Fedoniuk LYa, Nesteruk SO, Hnatiuk MS et al. Quantitative morphological features of the structural rearrangement of the venous blood vessels of the prostate gland in post-resection portal hypertension. *Pol Merkur Lekarski*. 2023;6(51):608-612. doi:10.36740/Merkur202306105. DOI 
28. Hnatiuk MS, Nesteruk SO, Fedoniuk LYa et al. Quantitative morphological analysis of age structural changes in prostate of experimental animals with ethanol poisoning. *Wiad Lek*. 2024;77(2):268-272. doi: 10.36740/WLek202402112. DOI 

CONFLICT OF INTEREST




The Authors declare no conflict of interest




CORRESPONDING AUTHOR


Oksana H. Popadynets




Ivano-Frankivsk National Medical University
2 Halytska St, 76000 Ivano-Frankivsk, Ukrainian
e-mail: Fedonyuk22Larisa@gmail.com

ORCID AND CONTRIBUTIONSHIP

Liliia V. Sobol: 0000-0002-9750-3493   

Ivan S. Kuibida: 0009-0007-1534-2213   

Oleksandra T. Harhaun: 0009-0004-1437-8941   

Oksana H. Popadynets: 0000-0002-2093-5984   

 – Work concept and design,  – Data collection and analysis,  – Responsibility for statistical analysis,  – Writing the article,  – Critical review,  – Final approval of the article

RECEIVED: 10.05.2025

ACCEPTED: 07.09.2025

